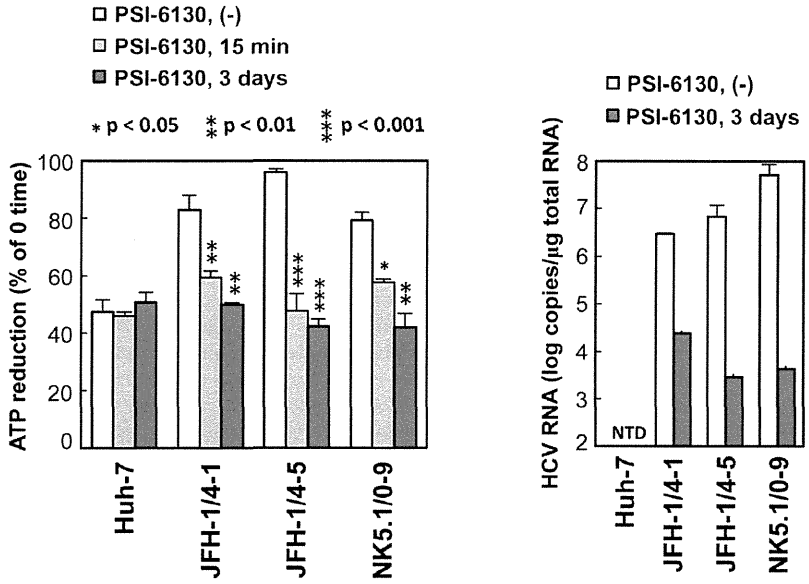

Figure 3. ATP consumption in cells replicating HCV RNA. (Left) The indicated cell lines were pretreated with 10 μM PSI-6130 for 3 days or were cultured in the absence of the drug, followed by trypsinization and permeabilization. ATP-containing reaction buffer plus 10 μM PSI-6130 was added to some of the non-pre-treated cells (PSI-6130, 15 min; light gray bars). ATP-containing PSI-6130-free reaction buffer was added to the rest of the non pre-treated cells (PSI-6130, (−); white bars) and to the pre-treated cells (PSI-6130, 3 days; dark gray bars). After 15 min incubation, ATP levels in cell lysates were measured using a luciferase-based assay. ATP reduction compared to ATP levels at the 0-time point was calculated. The mean values of three independent samples with SD are displayed. Statistical differences between cells treated with and without treatment with PSI-6130 were evaluated using Student's *t*-test. (Right) HCV RNA titers in cells corresponding to the left panel were determined using real-time quantitative RT-PCR. Data are presented as means and SD for three independent samples. NTD indicates not detected.
doi:10.1371/journal.ppat.1002561.g003

well as plasmids expressing NS5A-ATeam fusion proteins (NS5A-ATeam)(Figures 4A and 4C).

We first tested whether NS5A-ATeam fusion proteins can be used to monitor ATP levels over a range of concentrations in living cells. The Venus/CFP ratios in individual cells expressing NS5A fused either with AT1.03^{YEMK} (Kd = 1.2 mM at 37°C [2]) or with a relatively lower affinity version, AT1.03 (Kd = 3.3 mM at 37°C [2]) were measured. As shown in Figure 4B, differences in the Venus/CFP ratios of NS5A- AT1.03^{YEMK} and NS5A-AT1.03 were similar to those of AT1.03^{YEMK} and AT1.03, although average ratios were lower for NS5A- AT1.03^{YEMK} and NS5A-AT1.03 compared to AT1.03^{YEMK} and AT1.03. In the presence of 2DG and OliA, Venus/CFP ratios of NS5A-AT1.03^{YEMK} were markedly reduced to levels that were comparable to those of AT1.03^{RK}, an inactive mutant with R122K/R126K substitutions [2]. These results demonstrate that NS5A-ATeams can function as ATP indicators, although their dynamic ranges of Venus/CFP ratios are slightly smaller than those of the original, non-fused ATeams.

We next investigated whether the SGR-ATeam could initiate and sustain transient replication of HCV RNA in cells. A RNA polymerase I (Pol I)-derived plasmid, which carries SGR/luc-AT1.03 containing a luciferase reporter gene ([26]; Figure 4C), or its replication-defective mutant were transfected into Huh-7 cells and levels of viral replication were determined by measuring luciferase activity at various time intervals over a five day period (Figure 4D). Although replication of SGR/luc-AT1.03 was delayed compared with parental SGR/luc, the luciferase activity expressed from SGR/luc-AT1.03 rose to approximately a thousand-fold higher than that expressed from SGR/luc-GND-AT1.03 at five days post-transfection. It appears that SGR-AT1.03, which does not carry the luciferase gene, replicated more efficiently than SGR/luc-AT1.03, as determined by Western blotting of the HCV NS5B protein within cells four days post-transfection (Figure 4E). As indicated in Figure 4F, an abundant protein of the same size as that expected for the NS5A-ATeam fusion protein was observed in cells expressing either NS5A-AT1.03 or SGR-AT1.03, indicating that the NS5A-ATeam fusion protein is stable and is not cleaved during HCV replication. Thus, we concluded that the modified replicon constructs in which the ATeam is incorporated into the NS5A region are functional and remain capable of efficient transient replication of HCV RNA.

Visualization of ATP levels and distinctive features of ATP distribution in cells replicating ATeam-tagged SGR

This SGR-ATeam system that was established to analyze cellular ATP levels was used in living HCV RNA-replicating cells in which membrane-associated RCs are formed through the interaction of viral proteins, including NS5A, and cellular proteins. We compared the subcellular distribution of fluorescent signals expressed from NS5A-ATeams and SGR-ATeams using emission-scanning confocal fluorescence microscopy with a Zeiss META detector. NS5A-AT1.03 and NS5A-AT1.03^{YEMK} were diffusely distributed throughout the cytoplasm (Figure 5A; upper panels). Venus/CFP ratios of NS5A-ATeam constructs were almost constant throughout the cytoplasm (Figure 5A; lower). As expected, Venus/CFP ratios in cells expressing NS5A-AT1.03^{YEMK} were markedly higher than those of NS5A-AT1.03 (Figure 5A; lower). In contrast, cells replicating SGR-AT1.03 and SGR-AT1.03^{YEMK} showed foci of brightly fluorescent dot-like structures in the cytoplasm (Figure 5B; upper panels). Interestingly, some of these fluorescent foci had an apparently higher Venus/

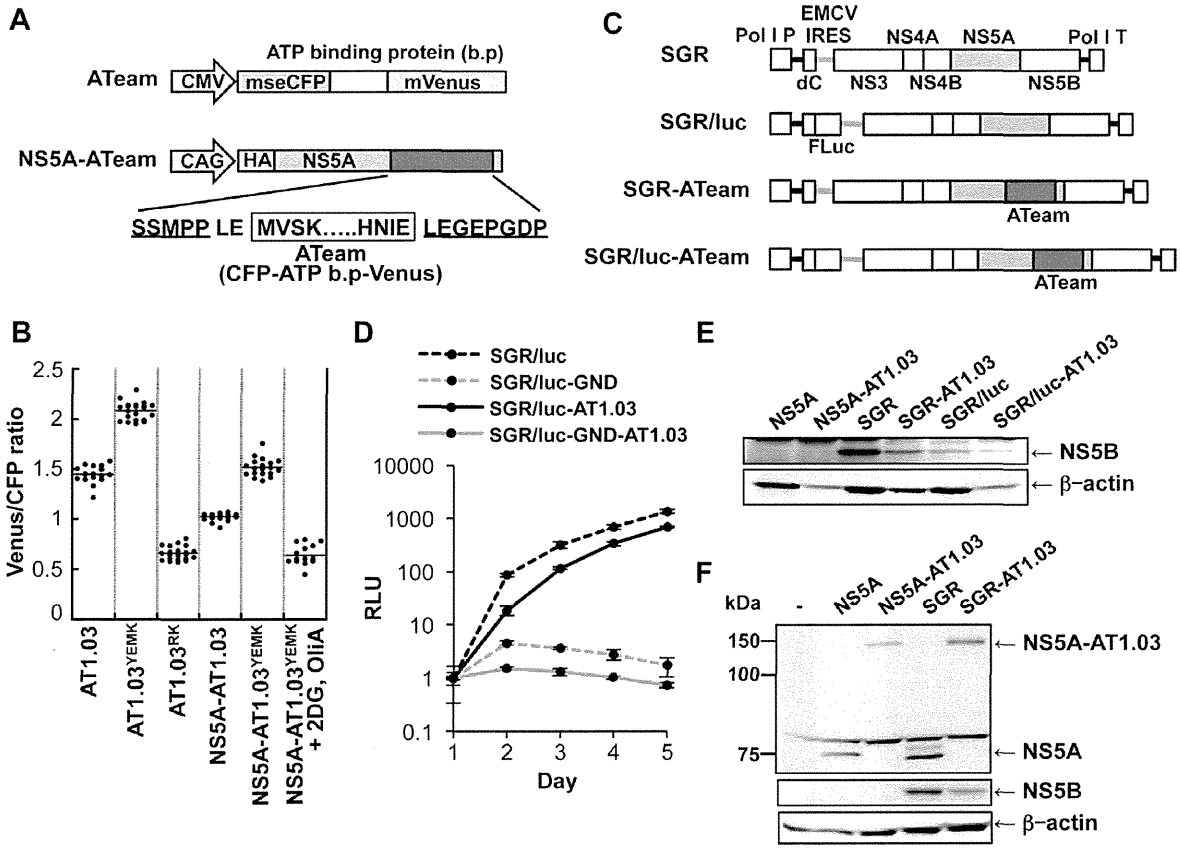

Figure 4. Development of NS5A-ATeam and SGR-ATeam to enable real-time monitoring of ATP. (A) Schematic representation of the ATeam and NS5A-ATeam used in this study. ATeam genes were inserted into the 3′ region of a HA-NS5A expression vector to generate NS5A-ATeam. The underlined sequences indicate NS5A residues. The insertion site was between residues 2394 and 2395, numbered according to the polyprotein of the HCV JFH-1 isolate. CMV, Cytomegalovirus promoter; CAG, CAG promoter; ATP b.p, ATP binding protein. HA, HA tag. (B) Huh-7 cells were transfected with ATeam and NS5A-ATeam constructs. Forty-eight hours post-transfection, the Venus/CFP ratios of each cell were calculated from fluorescent images acquired with a confocal microscope in the same way as described in the legends for Figure 2. Each plot shows the ratio of individual cells. Horizontal lines represent means. (C) Schematic representation of the SGR and SGR-ATeam plasmids used, with or without the firefly luciferase gene (Fluc). HCV polyproteins are indicated by the open boxes. ATeam genes were inserted into the same site in the NS5A C-terminal region. Bold lines indicate the HCV UTR. EMCV IRES is denoted by the gray bars. Pol I P, Pol I promotor; dC, 5′ region of Core gene; Pol I T, Pol I terminator. (D) Replication levels of SGR/luc-AT1.03 in transfected cells were determined by luciferase assay 1–5 days post-transfection. SGR/luc and SGR/luc-GND were used as positive and negative controls, respectively. Values given were normalized for transfection efficiency with luciferase activity determined 24 h post-transfection. All data are presented as means and SD for three independent samples. (E) Huh-7 cells were transfected with constructs encoding NS5A, NS5A-AT1.03, SGR, SGR-AT1.03, SGR/luc or SGR/luc-AT1.03, followed by immunoblotting with anti-NS5B or anti-beta-actin antibody. (F) Cells transfected with constructs encoding NS5A, NS5A-AT1.03, SGR or SGR-AT1.03 were analyzed by immunoblotting with anti-NS5A, anti-NS5B or anti-beta-actin antibodies.
doi:10.1371/journal.ppat.1002561.g004

CFP ratio than the surrounding cytoplasmic region (Figure 5B; middle and lower panels). Although the number of high Venus/CFP ratios was not consistent between the cells, this phenotype was observed in most of the cells that were replicating SGR-AT1.03 (Figure S3). Such high focal Venus/CFP ratios were not detected in cells replicating SGR-AT1.03^{RK} or in SGR-AT1.03^{YEMK} -replicating cells treated with 2DG and OliA. Thus, foci with a high Venus/CFP ratio apparently represent the presence of high ATP levels at distinct sites in cells replicating HCV RNA. In addition, when a replication-defective polyprotein that extended from NS3 through to the NS5B protein, including NS5A-AT1.03, was expressed, no high Venus/CFP ratio was seen in the cells in spite of the fact that NS5A-AT1.03 was detected in dot-like structures throughout the cytoplasm (Figure S4). These results strongly suggest that the high Venus/CFP ratios observed using the SGR-ATeam system are associated with the replication of HCV RNA.

To investigate whether the high Venus/CFP ratios of the dot-like structures detected in cells replicating SGR-ATeam are located at the HCV RC, FRET images of SGR-AT1.03-replicating cells were analyzed, followed immunofluorescence analysis of cells fixed and stained with either anti-NS5A or anti-NS3 antibodies (Figure 5C). Confocal fluorescence microscopy at high magnification demonstrated that the high Venus/CFP ratios that were identified in foci of various sizes were co-localized with NS5A and NS3 that were possibly membrane-bound within the cytoplasm of the viral replicating cells. Some of the NS3- or NS5A-labeled proteins that were identified by immunofluorescence were not associated with high Venus/CFP ratios. These results are consistent with previous reports, which demonstrated that only

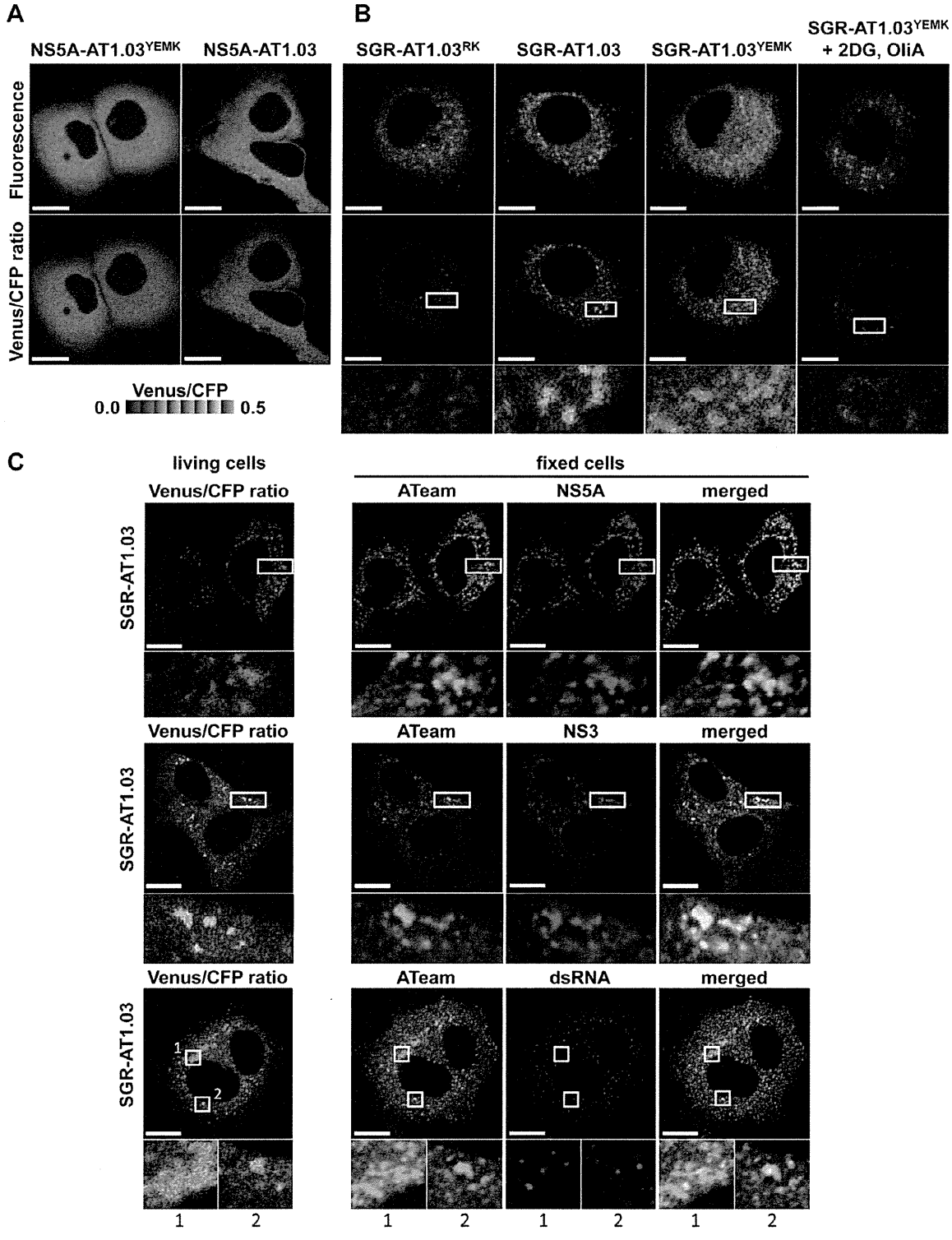

Figure 5. Visualization of sites of focal accumulation of ATP in cells expressing NS5A-ATeam or SGR-ATeam. (A) Huh-7 cells were transfected with NS5A-AT1.03 or NS5A-AT1.03^{YEMK}. Four days after transfection, the cells were analyzed using spectral imaging (405-nm excitation) of LSM510-META (Carl Zeiss). Images were processed to the CFP channel (F_{CFP}) and the Venus channel (F_{Venus}) using a linear unmixing algorithm using a reference for each spectrum. The upper panels demonstrate the signal intensity from a spectral channel with maximum intensity and represent the expression pattern of NS5A-ATeam. The lower panels are constructed from FRET ratio images (F_{CFP}/F_{Venus}) with pseudocolors. The pseudocolor scale is shown below. Scale bars, 20 μm. (B) Huh-7 cells were transfected with SGR-AT1.03^{RK}, SGR-AT1.03 or SGR-AT1.03^{YEMK}, and were analyzed in the same

way as described in (A). SGR-AT1.03^{YEMK} -transfected cells were treated with 10 mM 2DG and 10 μg/ml OliA just before imaging and were used as a negative control. The upper panels demonstrate the intensity from a spectral channel with maximum intensity and represent the expression pattern of NS5A-ATeam processed from SGR-ATeam. The lower panels indicate square areas within FRET ratio panels magnified five-fold. Scale bars, 20 μm. (C) Cells were fixed after live-cell FRET imaging, and the same cell was analyzed by indirect immunofluorescence staining. Viral proteins were labeled with antibodies against NS5A (upper panels), NS3 (middle panels) and dsRNA (lower panels), which were detected with an Alexa Fluor 555-labeled anti-rabbit or anti-mouse antibody. ATeam panels (green) represent the expression of NS5A-ATeam processed from SGR-ATeam, and NS5A, NS3 or dsRNA panels (red) represent the immunostained signals. Enlarged views of the areas outlined by squares at a five-fold magnification are also shown. Scale bars, 20 μm.
doi:10.1371/journal.ppat.1002561.g005

some of the expressed HCV NS proteins contribute to viral RNA synthesis [27]. To further investigate the relationship between the cellular sites at which there was a high Venus/CFP ratio and HCV RNA replication, double-stranded RNA (dsRNA) was visualized by staining with a specific anti-dsRNA antibody after FRET imaging (Figure 5C). This staining indicated that dsRNA-containing dot-like structures co-localized with structures that displayed high Venus/CFP ratios. Therefore, it is most likely that the dot-like structures with high Venus/CFP ratios that were detected using the SGR-ATeam system reflect the sites of HCV RNA replication or HCV RCs.

Several studies have shown that mitochondria, which play a central role in ATP metabolism, localize to areas near the membranous web, the likely site of HCV RNA replication [28]. We thus compared the subcellular localization of the fluorescence signals detected in cells expressing SGR-ATeam with that of mitochondria that were visualized by staining with Mitotracker. Foci with high Venus/CFP ratios did not colocalize with, but were localized adjacent to mitochondria in cells that were replicating SGR-AT1.03 (Figure S5). This finding might reflect the fact that ATP can be directly supplied from mitochondria to the sites of viral RNA replication in cells.

Quantification of ATP at putative cytoplasmic sites of HCV RNA replication within cells

Based on the above observations, FRET signals detected within cells expressing SGR-ATeam or NS5A-ATeam can be classified as either signals from distinct dot-like structures, which represent putative subcellular sites of HCV RNA replication, or as signals that are diffuse throughout the cytoplasm. The Venus/CFP emission ratio in individual cells into which NS5A-AT1.03, NS5A-AT1.03^{YEMK}, SGR-AT1.03, SGR-AT1.03^{YEMK} or SGR-AT1.03^{RK} was introduced was determined (Figure 6A). Fluorescent signals corresponding to cytoplasmic ATP were identified by subtracting signals at putative sites of viral RNA replication from signals from the cytoplasmic area as a whole. Cytoplasmic Venus/CFP ratios within cells replicating SGR-AT1.03 and SGR-AT1.03^{YEMK} were lower than those in cells expressing NS5A-AT1.03 and NS5A-AT1.03^{YEMK}, respectively. Therefore, cytoplasmic ATP levels within HCV RNA-replicating cells were lower than in non-replicating cells. This result is consistent with the findings shown in Figure 1A. The average Venus/CFP ratios at potential sites of viral RNA replication were greater than the corresponding cytoplasmic levels in cells replicating SGR-AT1.03 or SGR-AT1.03^{YEMK}. As expected, a significant decrease in Venus/CFP ratios was observed in cells treated with 2DG and OliA.

We next quantified ATP levels within individual cells replicating HCV RNA based on the Venus/CFP ratios obtained. To generate standard curves for this calculation, permeabilized cells expressing NS5A-AT1.03 or NS5A-AT1.03^{YEMK} were prepared by digitonin treatment, followed by the addition of defined concentrations of ATP and subsequent FRET analysis [29,30]. As shown in Figure 6B, under these experimental conditions, baseline Venus/CFP ratios of approximately 0.1 were detected in the absence of exogenous ATP, and Venus/CFP ratios were observed to increase linearly with increasing ATP concentration. The standard curves thus obtained can be used to estimate the ATP concentrations of unknown samples in which a particular ATeam containing an ATP probe at the C terminus of HCV NS5A, such as NS5A-ATeam or SGR-ATeam, have been introduced. Based on the fluorescent signal obtained in cells replicating SGR-ATeam, as well as in cells expressing NS5A-ATeam, the ATP concentration at putative sites of HCV RNA replication was estimated to be ~5 mM in the experiments shown in Figures 5A and 5B (average value of putative replication sites; 4.8 mM). After subtraction of the ATP that was localized at the HCV replication sites, the ATP concentration of HCV-replicating SGR cells (~1 mM) was found to be approximately half that observed in parental non-replicating cells (~2 mM)(average values in SGR and parental cells; 0.8 mM and 2.2 mM, respectively). To our knowledge, this is the first experiment in which ATP levels were estimated inside living cells during viral genome replication.

Figures 5 and 6A demonstrate changes in ATP concentrations at distinct sites in cells undergoing HCV RNA replication. Finally, we determined the effect of the PSI-6130 inhibitor of HCV replication on the change in subcellular ATP concentration in cells following introduction of SGR-AT1.03, SGR-AT1.03^{RK} or NS5A-AT1.03 (Figure 6C). In general, nucleoside analogue inhibitors of viral replication prevent RNA/DNA synthesis by chain termination immediately after addition to infected cells [23]. Indeed, as shown in Figure 3, a decrease in ATP consumption was detected even following a PSI-6130 treatment period as short as 15 min of permeabilized HCV replicon cells. We therefore analyzed and estimated ATP levels in cells in the presence of PSI-6130 for 10 min and 2 h. ATP concentrations at putative sites of viral RNA replication, as well as cytoplasmic ATP levels, were higher in SGR-AT1.03-replicating cells in the presence of 0.1–5 μM PSI-6130 for 10 min compared to the same cells without inhibitor treatment or to NS5A-AT1.03-expressing cells. A dose-dependent PSI-6130-induced increase in ATP levels at the putative replication sites was observed under the condition used. By treatment with PSI-6130 for 2 h, the ATP levels at putative replication sites were significantly lower than those without inhibitor treatment in SGR-AT1.03-replicating cells. The cytoplasmic ATP levels were similar with or without 2-h treatment (Figure 6C). In HCV SGR-ATeam cells treated with PSI-6130 for 3 days, HCV RNA replication was dramatically inhibited by greater than 90% with no observed cytotoxicity (Figure S6) and, as expected, little or no high Venus/CFP signal was detected anywhere in the cells (data not shown). We adapted the ATeam system to monitor ATP in HCV RNA replicating cells and found increased ATP levels at the putative subcellular sites of the viral replication. Findings obtained from experiments using the viral polymerase inhibitor strongly suggest that changes in ATP concentrations at the distinct sites observed depend on the viral RNA replication.

Discussion

This paper is the first to demonstrate changes in ATP within cells during viral genome replication. ATP requirements during

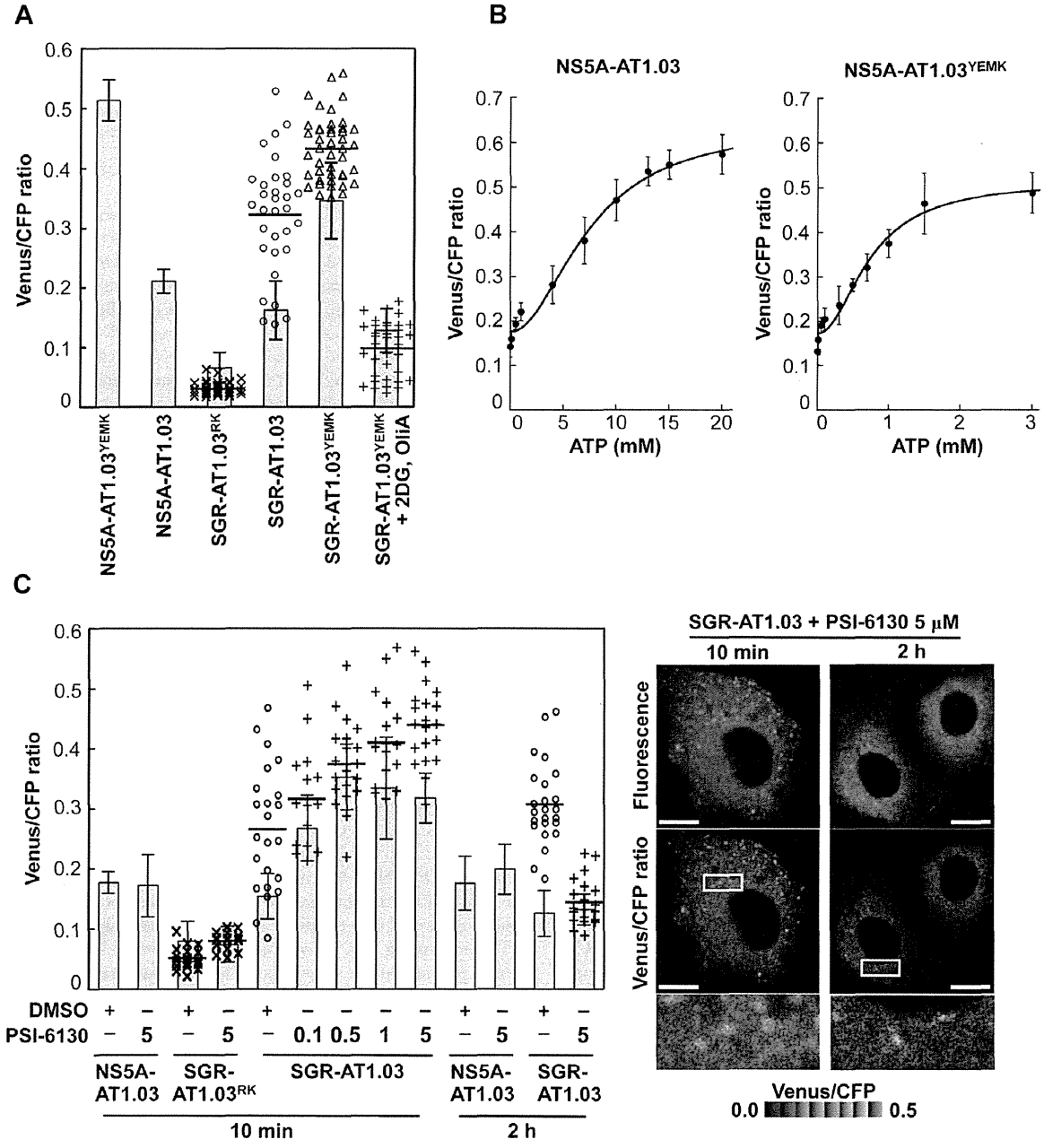

Figure 6. Estimation of ATP levels at possible sites of HCV RNA replication in living cells. (A) Venus/CFP emission ratios were calculated from images of CFP and Venus channels in individual cells for each group. Bar- and dotted graphs indicate ratios within the cytoplasm and ratios for dot-like structures, respectively, in the same cells, as shown in Figures 5A and 5B. Data in bar graphs are indicated as means and SD. Horizontal lines in the dot graphs denote means from at least three independent cells. Values in the cytoplasm of cells transfected with NS5A-AT1.03^{YEMK} and SGR-AT1.03^{YEMK} were statistically significant ($p<0.05$) as evaluated using the Student's *t*-test. (B) Calibration of NS5A-ATeam in cells under semi-intact conditions. Cells were transfected with NS5A-AT1.03 and NS5A-AT1.03^{YEMK}, respectively. Forty-eight hours later, the cells were permeabilized, followed by addition of known concentrations of ATP. FRET analyses were performed as described in Figure 5A. Each trace represents mean with SD of at least six independent cells. Plots were fitted with Hill equations with a fixed Hill coefficient of 2; $R=(R_{max}-R_{min})\times[ATP]^2/([ATP]^2+Kd^2)+R_{min}$, where R_{max} and R_{min} are the maximum and minimum fluorescence ratios, respectively. *Kd* is the apparent dissociation constant. R values were 0.994 and 0.986 for NS5A-AT1.03 and NS5A-AT1.03^{YEMK}, respectively. (C) Cells were transfected with NS5A-AT1.03, SGR-AT1.03^{RK} or SGR-AT1.03. The cells were then treated with PSI-6130 at indicated concentrations (μM) for 10 min or 2 h, and were analyzed as described in (A). Values in the cytoplasm of cells transfected with SGR-AT1.03 with and without PSI-6130 treatment were statistically significant ($p<0.05$ for control versus 0.1 or 1 μM PSI-6130, $p<0.01$ for control versus 0.5 or 5 μM PSI-6130) as evaluated using the Student's *t*-test. Representative cells treated with 5 μM PSI-6130 are shown in the right panel. The lower panel is a five-fold magnification of the boxed area. Scale bars, 20 μm.
doi:10.1371/journal.ppat.1002561.g006

the virus lifecycle have been studied for years. Several key steps during the viral life cycle, such as genome synthesis, require high-energy phosphoryl groups. For instance, it has been shown that ATP is required for the formation of a preinitiation complex for de novo RNA synthesis by RdRp of flaviviruses [31]. Transcriptional initiation and RNA replication by influenza virus RdRp are functional in an ATP-dependent fashion [32,33]. An ATP requirement of viral helicase activities has also been reported [34]. Furthermore, it has been demonstrated that ATP is involved in the assembly and/or release of viral structural proteins possibly via interaction with ATP-dependent chaperones [35,36]. However, it has been controversial as to whether ATP can be concentrated in particular subcellular compartment(s) in infected cells during viral replication. One of the underlying reasons for this controversy may be that a method by which cellular ATP levels can be determined, apart from examination of ATP levels in cellular extracts in the steady-state, has been lacking [37]. Recently Imamura et al. established FRET-based indicators, known as ATeams, for ATP quantification, and have shown that the use of ATeams enables the monitoring of ATP levels in real-time in different cellular compartments within individual cells [2].

In this study, in order to visualize and monitor ATP levels in living cells during replication of the viral genome, we first introduced the original ATeam-expressing plasmids into cells and found that cytoplasmic ATP levels in cells undergoing HCV genotype 1b and 2a RNA replication were lower than those in cured or parental cell lines (Figures 2 and S2). These results agree with the results of CE-TOF MS analysis (Figure 1) and the ATP consumption assay (Figure 3). It is therefore likely that ATP is actively consumed in cells during viral RNA replication, resulting in reduced levels of ATP in the cytoplasm. Furthermore, NS5A-ATeam fusion constructs, in which the ATeam gene was introduced into the C-terminal end of the NS5A coding region, and SGR-ATeam constructs containing a HCV JFH-1-derived subgenomic replicon within the NS5A-ATeam fused sequence as described above, were engineered (Figure 4). The results obtained using several ATeam fusion constructs with different affinities for ATP indicated that NS5A-ATeam fusion constructs can be used as FRET-based ATP indicators, and that the ATeam-tagged HCV replicons are capable of transient replication of viral RNA (Figure 4). It is interesting that our experiment using a SGR-ATeam construct provides evidence for the formation of ATP-enriched foci within cells that support HCV RNA replication (Figures 5 and 6). FRET-signal detection followed by indirect immunofluorescence allowed us to visualize co-localization of viral proteins as well as dsRNA at sites of ATP accumulation in cells (Figure 5), suggesting that these membrane-associated ATP-enriched foci likely represent sites of HCV RNA replication in transient replication assays.

Attempting to precisely quantify ATP within individual cells or particular intracellular compartments is a very challenging process. The luciferin-luciferase reaction has been utilized to monitor cellular ATP levels by measuring the released photon count during catalysis of bioluminescent oxidation by firefly luciferase. A previous study based on the luciferin-luciferase assay estimated basal cytoplasmic ATP levels at ~1.3 mM, which increased to ~5 mM during apoptotic cell death [38]. However, the results obtained were likely influenced by cellular levels of luciferase and other assay components, as well as by the pH of the cells. In this study, we describe quantification of ATP in human hepatoma Huh-7 cells undergoing HCV RNA replication using SGR-ATeam technology. Although ATP requirements during the lifecycles of various viruses have been studied for years, the use of ATeam technology enabled us, for the first time, to evaluate ATP concentrations at sites of viral replication within living cells. We here demonstrate that ATP concentrations at these putative subcellular sites of HCV RNA replication approach ~5 mM (Figure 6). This ATP level is as high as that observed during apoptotic processes such as caspase activation and DNA fragmentation, even though the latter ATP level was determined using a different assay system [38]. Considering that these apoptotic events were not observed at basal ATP levels [38], replication of the viral genome likely also requires high concentrations of cellular ATP. It should be noted that, in contrast to the fluorescent reporter system traditionally used to calculate the ATP/ADP ratio [39], the bacterial epsilon subunit used in ATeam is highly specific for ATP, but not for other nucleotides such as ADP, CTP, GTP or UTP [2,3]. In evaluating the effect of the HCV polymerase inhibitor on changes in the subcellular ATP concentration in cells replicating SGR-ATeam, an increase in ATP concentration was observed both at putative replication sites and in the cytoplasm of SGR-AT1.03-replicating cells in the presence of PSI-6130 for 10 min (Figure 6C). By contrast, 2-h treatment with the inhibitor resulted in reduction of ATP levels at putative replication sites in the replicon cells. Although the result of the experiment with 10-min treatment may be somewhat unexpected, it might possibly be explained by the following hypothesis. PSI-6130 began to inhibit viral RNA synthesis, leading to a decrease in ATP consumption. Since a mechanism for ATP transport mediated by host cell and/or viral factor(s) is still active during this time period, the ATP level at the replication sites should be increased compared to that during active replication. Higher levels of metabolic intermediates for glyconeogenesis as well as for glycolysis in HCV-infected cells compared to non-infected cells as determined via metabolome analysis (data not shown) may also be implicated in the increased ATP levels at the initial stage of inhibition of HCV replication. It is likely that active consumption of ATP caused by HCV replication and ATP transportation into the replication sites would lead to reduction of cytoplasmic ATP level. Such a change in ATP balance may result in induction of ATP generation and increase in certain metabolic intermediates related to glucose metabolism. These metabolome responses are supposed to maintain in short-term (10 min) treatment with PSI-6130. Thus, inhibition of HCV RNA replication by PSI-6130 under the conditions used may lead to increase in the cytoplasmic ATP level. It is likely that these metabolome responses were not observed after the longer-term (2 h) treatment presumably because the viral replication was inhibited by the inhibitor for a sufficient period of time. Further study is required to address the molecular mechanism underlying change in ATP balance caused by HCV replication and the viral inhibitors.

The mechanism by which ATP accumulates at potential sites of HCV RNA replication remains unclear. We have previously demonstrated that creatine kinase B (CKB), which is an ATP-generating enzyme and maintains cellular energy stores, accumulates in the HCV RC-rich fraction of viral replicating cells [22]. Our earlier results suggest that CKB can be directed to the HCV RC via its interaction with the HCV NS4A protein and thereby functions as a positive regulator for the viral replicase by providing ATP [22]. One may hypothesize that recruitment of the ATP generating machinery into the membrane-associated site, through its interaction with viral proteins comprising the RC, is at least in part linked with elevated concentrations of ATP at a particular site. Through our preliminary study, however, subcellular ATP distribution was not changed significantly in replicon cells where HCV RNA replication was reduced ~50% by siRNA-mediated knockdown of the CKB gene (data not shown). Another possibility

may be implication of communication between mitochondria and membrane-enclosed structures of HCV RC in ATP transport through membrane-to-membrane contact. As indicated in Figure S5, putative sites of the viral RNA replication with high Venus/CFP ratios were mainly localized proximal to mitochondria. Studies are ongoing to understand the mechanism(s) underlying this phenomenon, as well as to determine if changes in ATP levels at intracellular sites supporting replication might also be observed for other RNA or DNA viruses.

In summary, we have used a FRET-based ATP indicator called ATeam to monitor ATP levels in living cells where viral RNA replicates by designing HCV replicons harboring wild-type or mutated ATeam probes inserted into the C-terminal domain of NS5A. We evaluated changes in ATP levels during HCV RNA replication and demonstrated elevated ATP levels at putative sites of replication following detection of FRET signals, which appeared as dot-like foci within the cytoplasm. The ATeam system may become a powerful tool in microbiology research by enabling determination of subcellular ATP localization in living cells infected or associated with microbes, as well as investigation of the regulation of ATP-dependent processes during the lifecycle of various pathogens.

Materials and Methods

Chemicals

PSI-6130 (β-$_D$-2′-Deoxy-2′-fluoro-2′-*C*-methylcytidine) and recombinant human IFN-alpha2b were obtained from Pharmasset Inc. (Princeton, NJ) [23,24] and Schering-Plough (Kenilworth, NJ), respectively. OliA and 2DG were purchased from Sigma-Aldrich (St. Louis, MO). ATP used in this study was complexed with equimolar concentrations of magnesium chloride before use in the experiments.

Plasmids

The construction of the ATeam plasmids pRSET-AT1.03, pRSET-AT1.03^{YEMK} and pRSET-AT1.03$^{R122K/R126K}$, which express wild-type ATeam (AT1.03), as well as a high-affinity mutant (AT1.03^{YEMK}) and a non-binding mutant (AT1.03^{RK}), has been previously described [2]. pHH/SGR-Luc (also termed SGR/luc) contains cDNA of a subgenomic replicon of HCV JFH-1 isolate (genotype 2a; [14]) with firefly luciferase flanked by the Pol I promoter and the Pol I terminator, yielding efficient RNA replication upon DNA transfection [26]. pHH/SGR-Luc/GND (also termed SGR/luc-GND), in which a point mutation of the GDD motif of the NS5B was introduced in order to abolish RNA-dependent RNA polymerase activity, was used as a negative control. pHH/SGR (also termed SGR) was created by deleting the luciferase gene in pHH/SGR-Luc. To generate a series of SGR-ATeam plasmids, wild-type or mutant ATeam genes were inserted into pHH/SGR-Luc or pHH/SGR at the Xho I site of NS5A (between amino acids 418 and 419) [25]. The ATeam genes were also inserted into the same site of pCAGNS5A, which contains the NS5A gene of JFH-1 downstream of the CAG promoter and hemagglutinin (HA) tag [26], yielding NS5A-ATeam plasmids. To generate a plasmid expressing NS3-NS5B-AT1.03 under the control of the CAG promoter, a DNA fragment containing the coding region of NS3/NS4A/NS4B/NS5A-AT1.03/NS5B of SGR/luc-ATeam was inserted into the pCAGGS vector [40]. Exact cloning strategies are available upon request.

Cell culture and plasmid transfection

Human hepatoma Huh-7 cells were propagated in Dulbecco's modified Eagle's medium (DMEM) supplemented with 10% fetal calf serum (FCS) as well as minimal essential medium non-essential amino acid (MEM NEAA)(Invitrogen, Carlsbad, CA) in the presence of 100 units/ml of penicillin and 100 μg/ml of streptomycin. The Huh-7-derived cell lines JFH-1/4-1 and JFH-1/4-5, which support replication of SGR RNA of HCV JFH-1 (genotype 2a) and NK5.1/0-9, which carries the SGR RNA of Con1 NK5.1 (genotype 1b), were cultured and maintained under previously described conditions [15]. DNA transfection was performed using a TransIT-LT1 transfection reagent (Takara, Shiga, Japan) in accordance with the manufacturer's instructions.

CE-TOF MS analysis

Huh-7 cells were mock-infected or infected with HCVcc derived from a wild-type JFH-1 isolate at a multiplicity of infection of 1. When most cells had become virus positive, as confirmed by immunofluorescence, with no observable cell damage at 9 days post-infection, equal amounts of cells with and without HCV infection were scraped with MeOH including 10 μM of an internal standard after washing twice with 5% mannitol solution. Replicon cells (JFH-1/4-5) that were cultured in the absence of G418 for 2 days were harvested and prepared as above. The extracts were mixed with chloroform and water, followed by centrifugation at 2,300× *g* for 5 min at 4°C, The upper aqueous layer was centrifugally filtered through a 5-kDa cutoff filter to remove proteins. The filtrate was lyophilized and dissolved in water, then subjected to CE-TOF MS analysis. CE-TOF MS experiments were performed using an Agilent CE-TOF MS system (Agilent Technologies, Waldbronn, Germany) as described previously [41].

ATP consumption assay

The ATP consumption assay using permeabilized replicon cells was carried out as previously described [13,22] with slight modifications, so that it was unnecessary to add either exogenous phosphocreatine or creatine phosphokinase to minimize ATP reproduction in cells. Cells (2×10^6) cultured in the presence or absence of PSI-6130 for 72 h were treated with 5 μg Actinomycin D/ml, followed by trypsinization and 3 washes with cold buffer B (20 mM HEPES-KOH [pH 7.7], 110 mM potassium acetate, 2 mM magnesium acetate, 1 mM EGTA, and 2 mM dithiothreitol). The cells were permeabilized by incubation with buffer B containing 50 μg/ml digitonin for 5 min on ice and the reaction was stopped by washing 3 times with cold buffer B. The permeabilized cells (1×10^5) were resuspended with 100 μl buffer B containing 5 μM ATP, GTP, CTP, and UTP, 20 μM $MgCl_2$, and 5 μg/ml Actinomycin D. After incubation at 27°C for 15 min, samples were centrifuged, and 20 μl of the supernatant was then mixed with 5 μl of 5× passive lysis buffer (Promega, Madison, WI). The ATP level was determined using a CellTiter-Glo Luminescent cell viability assay system (Promega). All assays were performed at least in triplicate.

Live cell microscopy

Plasmids carrying the ATP indicators were transfected at 48 h (ATeam and NS5A-ATeam) or 4 days (SGR-ATeam) before imaging of the cells. One day before imaging, the cells were seeded onto 30-mm glass-bottomed dishes (AGC Techno Glass, Chiba, Japan) at about 60% confluency. For imaging, the cells were maintained in phenol red-free DMEM containing 20 mM HEPES-KOH [pH 7.7], 10% FCS and MEM NEAA.

Two kinds of confocal microscopies were used to perform the FRET analysis in this study as follows. Since the ways of acquisition of each spectrum were quite different between the two microscopies, differences in the values of the Venus/CFP ratios in different

experiments were observed. In Figures 2, 4B and S2, cells were imaged using a confocal inverted microscope FV1000 (Olympus, Tokyo, Japan) equipped with an oil-immersion 60× Olympus UPlanSApo objective (NA = 1.35). Cells were maintained on the microscope at 37°C with a stage-top incubation system (Tokai Hit, Shizuoka, Japan). Cells were excited by a 405-nm laser diode, and CFP and Venus were detected at 480–500 nm and 515–615 nm wavelength ranges, respectively. In the analysis shown in Figures 5, 6, S3, S4 and S5, FRET images were obtained using a Zeiss LSM510 Meta confocal microscope with an oil-immersion 63× Zeiss Plan-APOCHROMAT objective (NA = 1.4)(Carl Zeiss, Jena, Germany). Cells were maintained on the microscope at 37°C with a continuous supply of a 95% air and 5% CO_2 mixture using a XL-3 incubator (Carl Zeiss). Cells were excited by a 405-nm blue diode laser, and emission spectra of 433–604 nm wavelength range were obtained using an equipped scanning module (META detector) [42,43]. Images were computationally processed by a linear unmixing algorithm using the reference spectrum of CFP and Venus, which were obtained from individual fluorescence-expressing cells. All image analyses were performed using MetaMorph (Molecular Devices, Sunnyvale, CA). Fluorescence intensities of cytoplasmic areas in NS5A-ATeam transfected cells were calculated by subtraction of the signal intensities of the nucleus from the signal intensities of the whole cell, which was standardized by the area of the corresponding cytoplasmic region. Fluorescence intensities of cytoplasmic areas and at dot-like structures corresponding to the putative viral replicating sites in SGR-ATeam-transfected cells were measured and calculated as follows. All pixels above CFP intensity levels of 100–200 were selected. The positions of dot-like structures were then determined by examining areas greater than 0.5×10^{-12} square meters and the intensity of each dot was measured. The fluorescence intensity of the cytoplasmic area, excluding that of the putative viral replicating sites in each cell, was calculated by subtraction of the signal intensities of the nucleus and the dot-like structures, as determined above, from the signal intensity of the whole cell, which was standardized by the area of the corresponding cytoplasmic region. Each Venus/CFP emission ratio was calculated by dividing pixel-by-pixel a Venus image with a CFP image.

To investigate the relationship between Venus/CFP ratios and ATP concentrations in cells, calibration procedures were performed according to previous reports [29,30]. Huh-7 cells were transfected with NS5A-AT1.03 or NS5A-AT1.03^{YEMK}. Forty-eight hours later, the cells were permeabilized by incubation with buffer B containing 50 μg/ml digitonin for 5 min at room temperature. The reaction was stopped by washing 3 times with buffer B, followed by the addition of known concentrations of ATP in warmed medium for imaging. FRET analysis, with calibration of the signal intensity in the cytoplasm of each cell, was performed as described above. Plots were fitted with Hill equations with a fixed Hill coefficient of 2; $R = (R_{max}-R_{min})\times[ATP]^2/([ATP]^2+Kd^2)+R_{min}$, where R_{max} and R_{min} are the maximum and minimum fluorescence ratios, respectively and *Kd* is the apparent dissociation constant.

To analyze the effect of an inhibitor against HCV NS5B polymerase, the medium for the cells replicating SGR-ATeam was changed to medium containing various concentrations of PSI-6130. After 10-min incubation at 37°C under a continuous supply of 95% air and 5% CO_2, fluorescence intensities of cytoplasmic areas and at dot-like structures were determined as described above. Medium containing 0.01% DMSO was used as a negative control.

To visualize mitochondria, MitoTracker Red CMXRos (Molecular Probes, Eugene, OR) was added to the culture medium to a final concentration of 100 nM, incubated for 15 min at 37°C and the cells were then washed twice with phosphate buffered saline (PBS) before FRET analysis of living cells. Images were computationally processed as described above. The reference spectrum of MitoTracker Red CMXRos was obtained from stained parental, non-transfected, Huh-7 cells.

Indirect immunofluorescence

Cells expressing SGR-ATeam were cultured in 30-mm glass-bottomed dishes with an address grid on the coverslip (AGC Techno Glass). After FRET analysis of living cells as described above, the cells were fixed with 4% paraformaldehyde at room temperature for 30 min. After washing with PBS, the cells were permeabilized with PBS containing 0.3% Triton X-100 and individually stained with a rabbit polyclonal antibody against NS3 [44], an anti-NS5A antibody [45], or a mouse monoclonal antibody against dsRNA antibody (Biocenter Ltd., Szirak, Hungary) [46]. The fluorescent secondary antibody used was Alexa Fluor 555-conjugated anti-rabbit- or anti-mouse IgG (Invitrogen). The cells were imaged using a Zeiss LSM510 Meta confocal microscope with an oil-immersion 63× Zeiss Plan-APOCHROMAT objective (NA = 1.4). For dual-color imaging, the ATeam signal was excited with the 488-nm laser line of an argon laser and Alexa Fluor 555 was excited with a 543-nm HeNe laser under MultiTrack mode. Emission filters with a 505- to 530-nm band-pass and 560-nm-long pass filter were used.

Luciferase assay

Huh-7 cells transfected with SGR/luc or SGR/luc-ATeam were harvested at different time points after transfection (Figure 4D) or at 3 days after treatment with PSI-6130 (Figure S6) and lysed in passive lysis buffer (Promega). To monitor HCV RNA replication, the luciferase activity in cells was determined using a Luciferase Assay system (Promega). All assays were performed at least in triplicate.

MTT assay

Cell viability was assessed using the Cell Proliferation Kit II (Roche, Indianapolis, IN) according to the manufacturer's instructions. The kit measures mitochondrial dehydrogenase activity, which is used as a marker of viable cells, using a colorimetric sodium3′-[1(-phenylaminocarbonyl)-3,4-tetrazolium]-bis(4-methoxy-6-nitro)benzene sulfonic acid hydrate (MTT) assay.

Quantification of HCV RNA

HCV RNA copies in the replicon cells with or without PSI-6130 treatment were determined using the real-time detection reverse transcription polymerase chain reaction (RTD-PCR) described previously [47] with the ABI Prisom 7700 sequence detector system (Applied Biosystems Japan, Tokyo, Japan).

Western blotting

The proteins were transferred onto a polyvinylidene difluoride membrane (Immobilon; Millipore, Bedford, MA) after separation by SDS-PAGE. After blocking, the membranes were probed with a rabbit polyclonal anti-NS5A antibody [44], a rabbit polyclonal anti-NS5B antibody (Chemicon, Temecula, CA), or a mouse polyclonal anti-beta-actin antibody (Sigma-Aldrich), followed by incubation with a peroxidase-conjugated secondary antibody and visualization with an ECL Plus Western blotting detection system (GE Healthcare, Buckinghamshire, UK).

Supporting Information

Figure S1 ATP Levels in HCV replicon cells and parental Huh-7 cells determined by CE-TOF MS. ATP metabolites in Huh-7 cells and JFH-1/4-5 cells were measured by

CE-TOFMS. The values of each measurement are shown at left. The right graph shows means with SD of the data at left. Open bar; Huh-7 cells, gray bar; JFH-1/4-5 cells.
(TIF)

Figure S2 Cytoplasmic ATP levels in HCV replicon cells and IFN-treated cells. (Left) The HCV replicon cells JFH-1/4-1, JFH-1/4-5 (genotype 2a) and NK5.1/0-9 (genotype 1b), and parental Huh-7 cells were cultured for 72 h in the absence or presence of 1,000 IU/ml IFN-alpha. Forty-eight hours after transfection with AT1.03, the Venus/CFP emission ratio of each cell was calculated from fluorescent images acquired with the confocal microscope FV1000. All data are presented as means and SD for at least 10 independent cells. (Right) HCV RNA titers in cells corresponding to the left panel were determined using real-time quantitative RT-PCR. Data are presented as means and SD for three independent samples. NTD indicates not detected.
(TIF)

Figure S3 Increase in ATP-enriched dot-like structures in cells replicating SGR-ATeam. Huh-7 cells were transfected with SGR-AT1.03, and analyzed in the same way as described in the legends for Figures 5A and 5B. The lower four panels are five-fold magnifications of the boxed areas in independent cells. Scale bars, 40 μm.
(TIF)

Figure S4 Visualization of the ATP level in cells expressing replication-defective HCV polyprotein. (A) A schematic representation of the NS3-NS5B-AT1.03 plasmid is shown. The HCV polyprotein is indicated by the open boxes. The ATeam gene was inserted into the same site as that for NS5A-ATeam and SGR-ATeam insertion as indicated in the legend for Figure 4A. CAG, CAG promoter. (B) Cells transfected with constructs encoding NS5A, NS5A-AT1.03, NS3-NS5B-AT1.03, SGR or SGR-AT1.03 were analyzed by immunoblotting with anti-NS5A, anti-NS5B or anti-beta-actin antibodies. (C) Huh-7 cells were transfected with NS3-NS5B-AT1.03, and analyzed in the same way as described in the legends for Figures 5A and 5B. The upper panel (Fluorescence) demonstrates signal intensity from a spectral channel with maximum intensity and represents the expression pattern of NS5A-ATeam processed from NS3-NS5B-AT1.03. The lower panels (Venus/CFP ratio) indicate the FRET ratio and a five-fold magnification of the boxed area. Scale bar, 20 μm.
(TIF)

Figure S5 Relationship between ATP-enriched dot-like structures and mitochondria. Huh-7 cells replicating SGR-AT1.03 (right panels) and parental cells (left panel) were analyzed. Active mitochondria were labeled with MitoTracker Red CMXRos in living cells, and were analyzed in the same way as described in the legends for Figures 5A and 5B, using a reference for the MitoTracker spectrum. The lowest panels of SGR-ATeam cells indicate five-fold magnifications of the boxed areas. Scale bars, 20 μm.
(TIF)

Figure S6 Inhibitory effect of PSI-6130 on HCV RNA replication. (A) Replication levels of SGR/luc-AT1.03 RNA in transfected cells were determined by luciferase assay 3 days after treatment with PSI-6130 at the indicated concentrations (μM). The values shown were normalized for transfection efficiency with luciferase activity determined 24 h post-transfection. All data are presented as means and SD for three independent samples. (B) Cell viability was assessed using the MTT assay.
(TIF)

Acknowledgments

We are grateful to Minoru Tobiume, Tadaki Suzuki, Teruyuki Nagamune, Satoshi Yamaguchi, Yoshiharu Matsuura, Hiroto Kambara, Tomoko Date, Su Su Hmwe, Koichi Watashi, Takahiro Masaki and Takanobu Kato for their excellent technical assistance and advice, as well as to Takeharu Nagai for providing the mVenus expression vector and to Atsushi Miyawaki for providing the mseCFP expression vector. We thank our coworkers for their helpful discussions. We also thank Mami Sasaki for her technical assistance and Tomoko Mizoguchi for her secretarial work. We also thank the University of Tokyo Center for NanoBio Integration and the Department of Pathology in the National Institute of Infectious Diseases, Japan, for use of their confocal microscope.

Author Contributions

Conceived and designed the experiments: T. Ando, H. Imamura, T. Wakita, T. Suzuki. Performed the experiments: T. Ando, H. Aizaki. Analyzed the data: T. Ando, H. Imamura, T. Watanabe, T. Wakita, T. Suzuki. Contributed reagents/materials/analysis tools: H. Imamura, R. Suzuki, H. Aizaki. Wrote the paper: T. Ando, T. Suzuki.

References

1. Ranji A, Boris-Lawrie K (2010) RNA helicases: Emerging roles in viral replication and the host innate response. RNA Biol 7: 775–787.
2. Imamura H, Nhat KP, Togawa H, Saito K, Iino R, et al. (2009) Visualization of ATP levels inside single living cells with fluorescence resonance energy transfer-based genetically encoded indicators. Proc Natl Acad Sci U S A 106: 15651–15656.
3. Kato-Yamada Y, Yoshida M (2003) Isolated epsilon subunit of thermophilic F1-ATPase binds ATP. J Biol Chem 278: 36013–36016.
4. Iino R, Murakami T, Iizuka S, Kato-Yamada Y, Suzuki T, et al. (2005) Real-time monitoring of conformational dynamics of the epsilon subunit in F1-ATPase. J Biol Chem 280: 40130–40134.
5. Yagi H, Kajiwara N, Tanaka H, Tsukihara T, Kato-Yamada Y, et al. (2007) Structures of the thermophilic F1-ATPase epsilon subunit suggesting ATP-regulated arm motion of its C-terminal domain in F1. Proc Natl Acad Sci U S A 104: 11233–11238.
6. Bartenschlager R, Sparacio S (2007) Hepatitis C virus molecular clones and their replication capacity in vivo and in cell culture. Virus Res 127: 195–207.
7. Pezacki JP, Singaravelu R, Lyn RK (2010) Host-virus interactions during hepatitis C virus infection: a complex and dynamic molecular biosystem. Mol Biosyst 6: 1131–1142.
8. Suzuki T, Ishii K, Aizaki H, Wakita T (2007) Hepatitis C viral life cycle. Adv Drug Deliv Rev 59: 1200–1212.
9. Cai Z, Liang TJ, Luo G (2004) Effects of Mutations of the Initiation Nucleotides on Hepatitis C Virus RNA Replication in the Cell. J Virol 78: 3633–3643.
10. Moradpour D, Penin F, Rice CM (2007) Replication of hepatitis C virus. Nat Rev Microbiol 5: 453–463.
11. Dumont S, Cheng W, Serebrov V, Beran RK, Tinoco I, Jr., et al. (2006) RNA translocation and unwinding mechanism of HCV NS3 helicase and its coordination by ATP. Nature 439: 105–108.
12. Frick DN (2007) The hepatitis C virus NS3 protein: a model RNA helicase and potential drug target. Curr Issues Mol Biol 9: 1–20.
13. Miyanari Y, Hijikata M, Yamaji M, Hosaka M, Takahashi H, et al. (2003) Hepatitis C virus non-structural proteins in the probable membranous compartment function in viral genome replication. J Biol Chem 278: 50301–50308.
14. Wakita T, Pietschmann T, Kato T, Date T, Miyamoto M, et al. (2005) Production of infectious hepatitis C virus in tissue culture from a cloned viral genome. Nat Med 11: 791–796.
15. Miyamoto M, Kato T, Date T, Mizokami M, Wakita T (2006) Comparison between subgenomic replicons of hepatitis C virus genotypes 2a (JFH-1) and 1b (Con1 NK5.1). Intervirology 49: 37–43.
16. Mankouri J, Tedbury PR, Gretton S, Hughes ME, Griffin SD, et al. (2010) Enhanced hepatitis C virus genome replication and lipid accumulation mediated by inhibition of AMP-activated protein kinase. Proc Natl Acad Sci U S A 107: 11549–11554.
17. Nakashima K, Takeuchi K, Chihara K, Hotta H, Sada K (2011) Inhibition of hepatitis C virus replication through adenosine monophosphate-activated protein kinase-dependent and -independent pathways. Microbiol Immunol 55: 774–782.

18. Nagai T, Ibata K, Park ES, Kubota M, Mikoshiba K, et al. (2002) A variant of yellow fluorescent protein with fast and efficient maturation for cell-biological applications. Nat Biotechnol 20: 87–90.
19. Appleby TC, Anderson R, Fedorova O, Pyle AM, Wang R, et al. (2011) Visualizing ATP-dependent RNA translocation by the NS3 helicase from HCV. J Mol Biol 405: 1139–1153.
20. Cheng W, Arunajadai SG, Moffitt JR, Tinoco I, Jr., Bustamante C (2011) Single-base pair unwinding and asynchronous RNA release by the hepatitis C virus NS3 helicase. Science 333: 1746–1749.
21. Beran RK, Lindenbach BD, Pyle AM (2009) The NS4A protein of hepatitis C virus promotes RNA-coupled ATP hydrolysis by the NS3 helicase. J Virol 83: 3268–3275.
22. Hara H, Aizaki H, Matsuda M, Shinkai-Ouchi F, Inoue Y, et al. (2009) Involvement of creatine kinase B in hepatitis C virus genome replication through interaction with the viral NS4A protein. J Virol 83: 5137–5147.
23. Ma H, Jiang WR, Robledo N, Leveque V, Ali S, et al. (2007) Characterization of the metabolic activation of hepatitis C virus nucleoside inhibitor beta-D-2′-Deoxy-2′-fluoro-2′-C-methylcytidine (PSI-6130) and identification of a novel active 5′-triphosphate species. J Biol Chem 282: 29812–29820.
24. Murakami E, Bao H, Ramesh M, McBrayer TR, Whitaker T, et al. (2007) Mechanism of activation of beta-D-2′-deoxy-2′-fluoro-2′-c-methylcytidine and inhibition of hepatitis C virus NS5B RNA polymerase. Antimicrob Agents Chemother 51: 503–509.
25. Moradpour D, Evans MJ, Gosert R, Yuan Z, Blum HE, et al. (2004) Insertion of green fluorescent protein into nonstructural protein 5A allows direct visualization of functional hepatitis C virus replication complexes. J Virol 78: 7400–7409.
26. Masaki T, Suzuki R, Saeed M, Mori K, Matsuda M, et al. (2010) Production of infectious hepatitis C virus by using RNA polymerase I-mediated transcription. J Virol 84: 5824–5835.
27. Shi ST, Lee KJ, Aizaki H, Hwang SB, Lai MMC (2003) Hepatitis C Virus RNA Replication Occurs on a Detergent-Resistant Membrane That Cofractionates with Caveolin-2. J Virol 77: 4160–4168.
28. Gosert R, Egger D, Lohmann V, Bartenschlager R, Blum HE, et al. (2003) Identification of the Hepatitis C Virus RNA Replication Complex in Huh-7 Cells Harboring Subgenomic Replicons. J Virol 77: 5487–5492.
29. Palmer AE, Jin C, Reed JC, Tsien RY (2004) Bcl-2-mediated alterations in endoplasmic reticulum Ca2+ analyzed with an improved genetically encoded fluorescent sensor. Proc Natl Acad Sci U S A 101: 17404–17409.
30. Dittmer PJ, Miranda JG, Gorski JA, Palmer AE (2009) Genetically encoded sensors to elucidate spatial distribution of cellular zinc. J Biol Chem 284: 16289–16297.
31. Nomaguchi M, Ackermann M, Yon C, You S, Padmanbhan R (2003) De Novo Synthesis of Negative-Strand RNA by Dengue Virus RNA-Dependent RNA Polymerase In Vitro: Nucleotide, Primer, and Template Parameters. J Virol 77: 8831–8842.
32. Klumpp K, Ford MJ, Ruigrok RW (1998) Variation in ATP requirement during influenza virus transcription. J Gen Virol 79(Pt 5): 1033–1045.
33. Vreede FT, Gifford H, Brownlee GG (2008) Role of initiating nucleoside triphosphate concentrations in the regulation of influenza virus replication and transcription. J Virol 82: 6902–6910.
34. Frick DN, Lam AM (2006) Understanding helicases as a means of virus control. Curr Pharm Des 12: 1315–1338.
35. Gurer C, Hoglund A, Hoglund S, Luban J (2005) ATPgammaS disrupts human immunodeficiency virus type 1 virion core integrity. J Virol 79: 5557–5567.
36. Li PP, Itoh N, Watanabe M, Shi Y, Liu P, et al. (2009) Association of simian virus 40 vp1 with 70-kilodalton heat shock proteins and viral tumor antigens. J Virol 83: 37–46.
37. Dennis PB, Jaeschke A, Saitoh M, Fowler B, Kozma SC, et al. (2001) Mammalian TOR: a homeostatic ATP sensor. Science 294: 1102–1105.
38. Zamaraeva MV, Sabirov RZ, Maeno E, Ando-Akatsuka Y, Bessonova SV, et al. (2005) Cells die with increased cytosolic ATP during apoptosis: a bioluminescence study with intracellular luciferase. Cell Death Differ 12: 1390–1397.
39. Berg J, Hung YP, Yellen G (2009) A genetically encoded fluorescent reporter of ATP:ADP ratio. Nat Methods 6: 161–166.
40. Niwa H, Yamamura K, Miyazaki J (1991) Efficient selection for high-expression transfectants with a novel eukaryotic vector. Gene 108: 193–199.
41. Soga T, Ohashi Y, Ueno Y, Naraoka H, Tomita M, et al. (2003) Quantitative metabolome analysis using capillary electrophoresis mass spectrometry. J Proteome Res 2: 488–494.
42. Haraguchi T, Shimi T, Koujin T, Hashiguchi N, Hiraoka Y (2002) Spectral imaging fluorescence microscopy. Genes Cells 7: 881–887.
43. Ishii M, Ikushima M, Kurachi Y (2005) In vivo interaction between RGS4 and calmodulin visualized with FRET techniques: possible involvement of lipid raft. Biochem Biophys Res Commun 338: 839–846.
44. Murakami K, Kimura T, Osaki M, Ishii K, Miyamura T, et al. (2008) Virological characterization of the hepatitis C virus JFH-1 strain in lymphocytic cell lines. J Gen Virol 89: 1587–1592.
45. Inoue Y, Aizaki H, Hara H, Matsuda M, Ando T, et al. (2011) Chaperonin TRiC/CCT participates in replication of hepatitis C virus genome via interaction with the viral NS5B protein. Virology 410: 38–47.
46. Taguwa S, Kambara H, Omori H, Tani H, Abe T, et al. (2009) Cochaperone activity of human butyrate-induced transcript 1 facilitates hepatitis C virus replication through an Hsp90-dependent pathway. J Virol 83: 10427–10436.
47. Takeuchi T, Katsume A, Tanaka T, Abe A, Inoue K, et al. (1999) Real-time detection system for quantification of hepatitis C virus genome. Gastroenterology 116: 636–642.

C型肝炎ウイルス（HCV）による感染

田中純子　広島大学大学院　医歯薬学総合研究科　疫学・疾病制御学
小山富子　岩手県予防医学協会　医療技術部
相崎英樹　国立感染症研究所　ウイルス二部

1. はじめに

ウイルス性肝炎の病因ウイルスの1つであるC型肝炎ウイルス（HCV）は，1989年に米国のHoughtonらによりHCV遺伝子の一部がクローニング[1]された比較的新しいウイルスである．1990年代は，急速に世界中でその測定系の開発と普及が推進されたことにより，さまざまな集団における肝炎ウイルス検査や調査等が広く行われ，徐々にC型肝炎ウイルス感染の状況が明らかになってきた．1992年以前，すなわち，C型肝炎ウイルス関連抗体検査(HCV抗体検査)が輸血用血液のスクリーニングとして普及・導入され始める以前には，世界中の輸血後肝炎の主な原因はC型肝炎ウイルスであったことをWHO(World Health Organization）は報告[2]している．また，HCVキャリア率は平均で3.0%，世界中のHCVキャリア数は1.3億人から1.7億人であると推計している．

本稿では，わが国におけるC型肝炎ウイルスによる感染状況(prevalence)を示すとともに，新規感染率（incidence）を垂直感染（母子感染）および水平感染に分けて成績を示す．

2. C型肝炎ウイルス（HCV）について

ウイルス性肝炎は，経口感染による伝染性肝炎と血液を介して感染する血清肝炎に大きく二分できる．経口感染による伝染性肝炎の病因ウイルスには，A型肝炎ウイルス（HAV：ピコルナウイルス科ヘパトウイルス属RNAウイルス）とE型肝炎ウイルス（HEV：ヘペウイルス科ヘペウイルス属RNAウイルス）があり，感染したヒトの糞便中に検出され，これに汚染された飲料水・食物を摂取することによって感染する．一方，血清肝炎の病因ウイルスには，B型肝炎ウイルス（HBV：ヘパドナウイルス科オルソヘパドナウイルス属DNAウイルス），C型肝炎ウイルス（HCV：フラビウイルス科ヘパシウイルス属RNAウイルス），D型肝炎ウイルス（HDV：サテライトウイルス科）があり，感染したヒトの血液中や微量な血液が混じった体液に検出されるが，これらの血液や体液がヒトの血液に入ることによって感染が起こる．D型肝炎ウイルス（HDV）はHBVをヘルパーウイルスとして増殖する特殊なウイルス（不完全ウイルスdefective virus）でありHDV単独での感染はなく，日本では稀である．

C型肝炎ウイルス（HCV）は，直径55～57nmの球形をしたRNA型ウイルスである．ウイルス粒子は二重構造をしており，ウイルスの遺伝子（RNA）とこれを包んでいるヌクレオカプシド（コア粒子），そして，これを被う

Prevalence of hepatitis C virus infection and incidence of vertical and horizontal hepatitis C virus infection in Japan
Junko TANAKA, Department of Epidemiology, Infectious Disease Control and Prevention, Graduate School of Biomedical Sciences, Hiroshima University
Tomiko KOYAMA, Division of Medical Technology, Iwateken Yobouigakukyoukai Inc. (Iwate Association of Preventive Medicine)
Hideki AIZAKI, Department of Virology II, National Institute of Infectious Diseases (NIID)
別刷請求先：田中純子　〒734-8551　広島市南区霞1-2-3　広島大学大学院医歯薬学総合研究科
Tel：082-257-5161　Fax：082-257-5164　E-mail：jun-tanaka@hiroshima-u.ac.jp

外殻（エンベロープ）から成り立っている．

C型肝炎ウイルスの抗体，すなわちHCV抗体とは，HCVのコア粒子に対する抗体（HCVコア抗体），エンベロープに対する抗体（E2/NS-1抗体），HCVが細胞の中で増殖する過程で必要とされるタンパク（非構造タンパク）に対する抗体（NS抗体：C100-3抗体，C-33c抗体，NS5抗体など）のすべてを含む総称となっている．

HCV抗体陽性者には，HCVに持続感染している例とウイルスがすでに排除された感染既往例とが混在している．1992年から献血時のスクリーニング検査に用いられていたHCV抗体測定系（凝集法，HCV PHA法，又はHCV PA法）では，この方法により陽性と判定された場合，その約70％がHCV RNA陽性（C型肝炎ウイルス持続感染者：HCVキャリア）であることが過去に行った基礎的調査により明らかになっている（なお，2008年5月末より日赤血液センターではHCV抗体測定はCLEA法により行われている）．

3. 肝癌による死亡の推移とその成因

人口動態統計[3]資料から得た肝癌による死亡の推移を図1に，またそのうちC型肝炎ウイルス（HCV）の持続感染に起因する死亡の割合について，人口動態統計資料と日本肝癌研究会による調査成績[1]を元に試算したものを図2に示す．

まず，悪性新生物「肝」(肝および肝内胆管の悪性新生物，人口動態統計，2009年）による死亡は，肺癌，胃癌に次いで，第3位と上位を維持し，死亡実数は32,725人（26.0/人口10万人対）と前年2008年（33,665人，26.7/人口10万人対）と比べやや死亡数は微減したが依然として3万人を超えている（図1）．

肝癌による死亡は，1950年代初めから1970年代半ばまでは人口10万人あたり10人前後（死亡実数は1万人以下）であったが，増加を始め2002年にピーク（人口10万人対27.5）を示した後，漸く横ばいとなっている．男性は，女性の肝癌による死亡の約2倍を示す高値（男性35.3，女性17.2/人口10万人対）であり，2002年以後には若干の減少傾向が認められるが，女性では現在に至るまで微増を続けている．

図2は，人口10万人あたりの肝細胞癌による死亡の推移とその病因別にみた内訳を試算したものである．

1975年以後，肝細胞癌による死亡数は増加しているが，HBVの持続感染に起因すると考えられる死亡の割合は人口10万人対5前後の一定値を示し増減がないまま推移している．すなわち，1970年代から2000年にかけて肝細胞がんによる死亡の増加は非A非B型によるものであっ

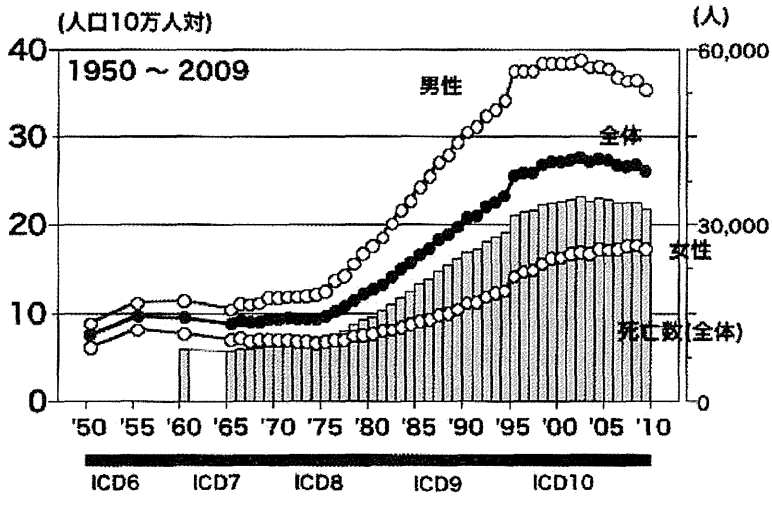

図1　わが国における肝がんによる死亡の推移

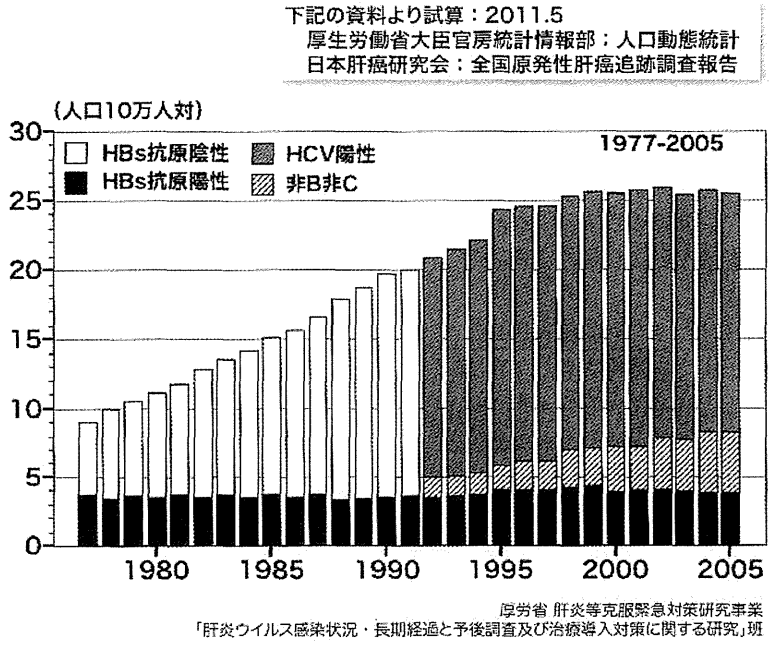

図２　病因別にみた肝がんによる死亡数の経年的推移

たことがわかる．1992年以降，HCV 感染の診断が可能となると図２のようにそのうちの約90％がHCV の持続感染に起因するものであったことが見て取れる．一方，2000年以降，非Ｂ非Ｃ型に由来する肝細胞癌による死亡割合が増加傾向にあることが明らかとなり，その原因や動向について NASH(Non-alcoholic steatohepatitis) との関連性が示唆されている．しかし，わが国の肝細胞がんによる死亡の約７割はHCV の持続感染に起因するものであり，肝癌対策を構築する上でも，HCV 持続感染者（HCV キャリア）の規模の把握や HCV 感染予防対策が重要と考えられる．

4．HCV キャリア率の把握（Prevalence）

4-1．一般集団における HCV キャリア率

HCV 持続感染者（HCV キャリア）の規模の把握を試みるために，2000年以後に得られた大規模集団，すなわち初回供血者集団と節目検診受診者集団から一般集団における年齢階級別にみたHCV キャリア率（prevalence）を算出しホす．

日本赤十字血液センターの献血時のスクリーニング検査は，輸血用血液の安全性確保のために行われるものであり，全国一律の基準，同一の試薬を用いて精度を維持し判定されている．また，2002年から５ヶ年計画で実施に移された節目・節目外検診は，老人保健法の住民検診に組み込まれた形で，公的補助により肝炎ウイルス検査（Ｃ型肝炎ウイルス検査，Ｂ型肝炎ウイルス検査）が行われたものであり，全国統一の検査手順に従って判定されたものである．

いずれも，自身が肝炎ウイルスに感染していることがわかっている場合は，献血や検診の対象者にはならないと考えられることから，この２つの集団から得られたHCV キャリア率は，感染を知らずにいる感染者の割合を示している．

また，初回供血者集団はその約85％が40歳未満の年齢であり，また，節目検診受診対象者は40歳以上の年齢層であることから，40歳未満の年齢層における HCV キャリア率については初回供血者集団の資料を，40歳以上の年齢層における HCV キャリア率は節目検診受診者集団の資料を用いた．

すなわち，2001年から2006年の全供血者のうち「初回供血者」3,748,422人の資料を抽出し，20～39歳（2005年時点の年齢換算）のHCV抗体陽性率に70％を乗じた値をHCVキャリア率とした．また，厚生労働省「肝炎ウイルス検診」の「節目検診受診者」6,204,968人の成績を用いて40～74歳のHCVキャリア率を算出した（図3）[5]．

全国8地域別，5歳刻みの年齢階級別HCVキャリア率を図3に示す．HCVキャリア率は，8地域ともに高年齢層において高い値を示し，20歳代以下の若年層では0.2％以下の極めて低い値を示す傾向が認められている．また，肝発がん年齢と考えられる60歳以上の高年齢集団のHCVキャリア率は，関東以西の地域，すなわち北陸東海（1.9％），近畿（2.1％），中国（1.7％），四国（2.0％）の地域では，北海道（1.1％）や東北地域（0.9％）と比較して高い値を示していることがわかる．

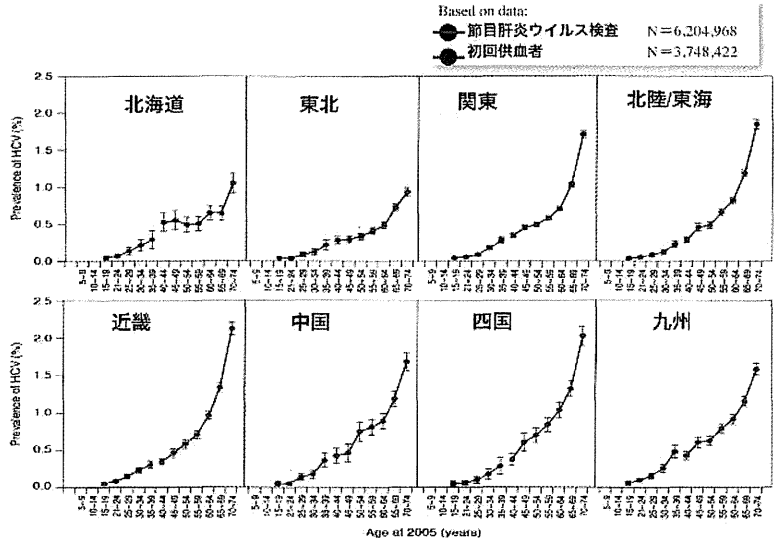

図3　地域別年齢階級別にみたHCVキャリア率

表1　出生年別にみた小学生でのHCV感染率
岩手県予防医学協会

出生年	対象数	HCV抗体陽性数（%）	小計
1978	2,429	4　(0.16)	
1979	4,180	4　(0.10)	
1980	3,538	6　(0.17)	HCV抗体陽性数
1981	2,512	3　(0.12)	24/26,996(0.09)
1982	1,591	1　(0.06)	
1983	1,088	0　(0.00)	HCV RNA陽性数
1984	5,991	4　(0.07)	Not Done
1985	5,667	2　(0.04)	
1986	6,775	2　(0.03)	HCV抗体陽性数
1987	6,505	6　(0.09)	26/32,049(0.08)
1988	6,310	10　(0.16)	
1989	6,436	5　(0.08)	HCV RNA陽性数
1990	6,023	3　(0.06)	7/32,049(0.02)
合計	59,045	50　(0.08)	

4-2. 児童におけるHCVキャリア率

岩手県予防医学協会がとりまとめた小学校入学時の調査成績を表1に示す．HCV抗体陽性率は，いずれの出生年においても0.1%あるいは0.1%以下の極めて低い値を示していることがわかる．ただし，節目検診の成績からみたHCVキャリア率を都道府県別にみると，岩手県は全国でも低率の県にあたることから，岩手県の調査成績がそのまま全国の児にあてはまるとはいえない．しかし，20歳以下の年齢層におけるHCVキャリア率は前項で示したように全国いずれの地域においても低いことから，他の地域における児童のHCVキャリア率も同様に低い値であることが推察される．

なお，HBV母子感染防止事業は1986年以後に出生したすべての児を対象に全国規模で実施されているが，HCV抗体陽性率/HCVキャリア率に関しては1986年を境にした前後の2つの期間に出生した児の集団間の差は認められていない．

5. HCV感染のリスク（Incidence）

感染の広がりを示すprevalenceについては，地域別あるいは年齢別のHCVキャリア率あるいはHCV抗体陽性率からその概要を示した．次に，感染のリスクを示すincidenceについて，これまでの疫学的調査結果をもとに，水平感染と母子感染の項を分けて示す．

5-1. 水平感染について

水平感染によるHCV新規発生について前向き調査を行った成績を表2に示す．

供血者集団を対象とした調査では，広島県赤十字血液センターにおける1994年6月から2004年4月までの供血者418,269人（総献血本数1,409,465本）を対象として前向きに観察し[6]，新たな感染の有無について解析を行ったところ，期間内に複数回献血をした218,797人（861,842人年）のうち新たなHCV感染が確認されたのは16例であり，人年法による解析でHCV新規発生率は10万人年あたり1.86人（95% CI：1.06～3.01人/10万人年）と示された．この成績は，同様の調査を1992年から3年間の観察期間で行った結果（1.8/10万人年，95% CI:0.4～5.2人/10万人年）とほぼ同じ値であった[7]．一方，女性のHCV新規発生率は2.77人/10万人年（95% CI：1.38～4.95人/10万人年）と，統計学的な有意差は認められなかったが，男性（1.08人/10万人年（0.35～2.51人/10万人年））

表2　HCV感染の新規発生率　1988～2004

	対象者	新規感染	観察人年	新規感染率　95% CI Incidence Rate
●供血者【広島】				
1992～1995	114,266	3	168,479	1.8/10万人年 0.4～5.2
1994～2004	218,797	16	861,842	1.9/10万人年 1.1～3.0
●供血者【大阪】				
1992～1997	448,020	59 ※抗体陽転	1,095,668	5.4/10万人年 4.1～7.0
●定期健康診断受診者【広島】				
1992～1995	3,079	0	5,786	0/10万人年 0～0.6
●障害者・老人福祉施設入所者【静岡】				
1988～1992	678	0	2,712	0/10万人年 0～1.3
●血液透析施設【広島】				
1999～2003	2,744	16	4,893	3.3/1000人年 1.7～4.9

のHCVキャリア妊婦から生まれた87児のうち，６ヶ月時点で感染が確認されたのは２例（2.3%）であった．２例の母親の出産時のHCV RNA量は1.0×10^7 Eq /ml(bDNA)，2.3×10^7 Eq /ml(bDNA）と高く，genotypeは母子共にそれぞれ2a，1bであり，児は24ヶ月，12ヶ月時点でHCV RNAが検出され感染が確認されている．

一方，HCV母子感染率の頻度に関する他の調査成績から報告された値は，調査地域や対象妊婦の背景因子の相異などにより２～10%と幅が大きい[12,13]．また，感染が確認された児の同胞すべてが感染成立したとはいえず，分娩方法や児の免疫能，出産時の母体のHCV RNA量などが関与していることが示唆されている．諸外国における調査報告からは，母親がHIV-HCV重複感染の場合のHCV母子感染率は高いことが明らかとなっているが，HCV単独感染の場合の母子感染率は低いことから，わが国では公的補助によるHCVの母子感染予防措置は行われていない．

6. 感染症法によるC型急性肝炎の発生状況について（相崎）

わが国では1999年４月に施行された感染症法により，急性のウイルス性肝炎を診断した医師は全例保健所へ届け出ることが必要になった．C型急性肝炎は，５類感染症に分類されており，届け出に基づいた集計解析は国立感染症研究所において行われている．

1999年４月から2009年12月までに届け出されたC型急性肝炎723例について[14]まとめたものを紹介する．1999年以来，急性C型肝炎と診断され報告された年別の患者数は，1999年136症例，2000年119症例，2001年65症例と2001年までは減少傾向が認められたが，それ以降2009年まで年間約30～70症例でほぼ横ばいに転じており，男女別に相異は認められていない．年齢階級別にみた報告数の分布では，30代前半及び50代後半の２つのピークが認められるが，14歳以下の小児または90歳以上の高齢者の報告は極めて少ない．男女別にみると，30代前半及び50代後半にみられる報告数のピークは女性で認められており，背景に感染の要因が潜在していることが推察される．都道府県別にみると，大都市部である大阪（125例），東京都（55例）等の報告数が多い一方，報告数がゼロの都道府県もありC型急性肝炎発生率には地域差が認められるが，報告義務の履行状況が地域ごとに異なる可能性もあり，発生数（率）の評価には注意が必要である．

2006年４月以降に報告されたC型急性肝炎167例について，感染の「原因不明」が全体の62%を占め，HCV感染原因は特定しにくいことが示されている．そのほかの感染原因として報告されたのは，針等刺入（22%），性的接触（11%）であった．また，報告総数は少ないが全体の22%を占める「針等刺入」の内訳では，針刺事故など医療行為に伴う感染以外に，ピアス，刺青，カミソリの共用，覚醒剤など，と報告されている．

医師の届け出義務の周知を広く徹底すると共に，得られる情報を適切に予防対策や啓蒙活動に取り入れることが求められている．

7. おわりに

わが国の社会生活全般における水平感染の発生要因が急速に消滅し，新規感染が低下した結果，若い世代におけるHCV抗体陽性率/HCVキャリア率は低い値を示すに至っている．わが国では「肝炎対策基本法」(2009年12月）を基盤として，すでに感染しているキャリアへの対策，具体的には，肝炎ウイルス検査の推進，肝疾患診療ネットワークの構築，新規治療法の開発等が積極的に進められている．

さまざまな機会で肝炎ウイルス検査が行われることにより感染を知る機会が増えたことで，感染を知らないままでいるHCVキャリア数は2005年時点，約81万人と推計し[15]，2000年時の推計値と比較して減少したと示した．一方で，感染していることを知ったがさまざまな理由から医療機関への受診をしないままでいるHCVキャリアや医療機関への継続受診に至っていないHCVキャリアが増加していることが問題点として指摘されている[16]．

世界的にみても肝炎対策先進国であるわが国は，これまでの感染防止策を継続しつつ，肝炎肝がん対策の新たな局面を迎えていると考えら

れる.

参考文献

1) Choo QL, Kuo G, Weiner AJ, Overby LR, Bradley DW, Houghton M : Isolation of a cDNA clone derived from a blood-borne non-A, non-B viral hepatitis genome. Science 244 : 359-362, 1989
2) World Health Organization. Hepatitis C. (Fact sheet N164. Updated June 2011 (http://www.who.int/mediacentre/factsheets/fs164/en/index.html))
3) 厚生労働省大臣官房統計情報部：平成21年人口動態統計　上巻, 2009
4) 日本肝癌研究会：第5回～第18回全国原発性肝癌追跡調査報告. 日本肝癌研究会事務局, 1982-2009
5) Tanaka J, Koyama T, Mizui M, Katayama K, Matsuo J, Akita T, Nakashima A, Miyakawa Y, Yoshizawa H : Total Numbers of Undiagnosed Carriers of Hepatitis C and B Viruses in Japan Estimated by Age- and Area-specific Prevalence on the National Scale. Intervirology 54 : 185-195, 2011
6) Tanaka J, Mizui M, Nagakami H, Katayama K, Tabuchi A, Komiya Y, Miyakawa Y, Yoshizawa H : Incidence rates of hepatitis B and C virus infections among blood donors in Hiroshima, Japan, during 10 years from 1994 to 2004. Intervirology 51 : 33-41, 2008
7) Sasaki F, Tanaka J, Moriya T, Katayama K, Hiraoka M, Ohishi K, Nagakami H, Mishiro S, Yoshizawa H : Very low incidence rates of community-acquired hepatitis C virus infection in company employees, long-term inpatients, and blood donors in Japan. J Epidemiol 6 : 198-203, 1996
8) Tanaka H, Tsukuma H, Hori Y, Nakade T, Yamano H, Kinoshita N, Oshima A, Shibata H : The risk of hepatitis C virus infection among blood donors in Osaka, Japan. J Epidemiol 8 : 292-296, 1998
9) Kumagai J, Komiya Y, Tanaka J, Katayama K, Tatsukawa Y, Yorioka N, Miyakawa Y, Yoshizawa H : Hepatitis C virus infection in 2,744 hemodialysis patients followed regularly at nine centers in Hiroshima during November 1999 through February 2003. J Med Virol 76 : 498-502, 2005
10) Nagata I, Shiraki K, Tanimoto K, Harada Y, Tanaka Y, Okada T : Mother-to-infant transmission of hepatitis C virus. J Pediatr 120 : 432-434, 1992
11) Moriya T, Sasaki F, Mizui M, Ohno N, Mohri H, Mishiro S, Yoshizawa H : Transmission of hepatitis C virus from mothers to infants : its frequency and risk factors revisited. Biomed Pharmacother 49 : 59-64, 1995
12) Okamoto M, Nagata I, Murakami J, Kaji S, Iitsuka T, Hoshika T, Matsuda R, Tazawa Y, Shiraki K, Hino S : Prospective reevaluation of risk factors in mother-to-child transmission of hepatitis C virus : high virus load, vaginal delivery, and negative anti-NS4a antibody. J Infect Dis 182 : 1511-1514, 2000
13) 白木和夫：HCV母子感染に関する研究. 厚生省非A非B型肝炎研究班, 平成7年度報告書：33-36, 1995
14) 相崎英樹：1999年から2009年における日本のC型急性肝炎の発生状況. 厚生労働省　肝炎等克服緊急対策研究事業「肝炎ウイルス感染状況・長期経過と予後調査及び治療導入対策に関する研究」(研究代表者　田中純子) 平成22年度　研究報告書：28-31, 2011
15) Tanaka J, Koyama T, Mizui M, Katayama K, Matsuo J, Akita T, Nakashima A, Miyakawa Y, Yoshizawa H. Total Numbers of Undiagnosed Carriers of Hepatitis C and B Viruses in Japan Estimated by Age- and Area-specific Prevalence on the National Scale. Intervirology 54 : 185-195, 2011
16) 田中純子：肝炎ウイルス感染状況・長期経過と予後調査及び治療導入対策に関する研究. 厚生労働省　肝炎等克服緊急対策研究事業「肝炎ウイルス感染状況・長期経過と予後調査及び治療導入対策に関する研究」平成22年度　総括報告書：1-27, 2011

細胞生物学講座

【C型肝炎ウイルスの生活環】

Title □□□□□□□□□□□□□□□□□□□□□□□□□□□□□

相崎　英樹

Hideki Aizaki

Key words

C型肝炎ウイルス，生活環，
脂質，脂肪滴

要　約

本原稿執筆にあたり，前回2001年10月に執筆させていただいた本誌を紐解いたところ，「HCVの研究はHCV cDNAの発現産物の解析による人工的なものばかりであり，ウイルス本来の性状やウイルスの生活環はわかっておらず，HCV増殖が効率良く観察できる細胞培養系の確立が最重要研究課題である」と記述していた。2005年に，JFH-1株のゲノムRNAをHuh-7細胞に導入することにより，感染性ウイルス粒子を効率良く作製する技術が確立された。これにより，HCVの生活環のすべてを再現可能な実験系が確立したことになり，HCV研究は目覚ましい進歩を遂げている。その結果，C型肝炎の治療法もインターフェロン中心の治療から，NS5A阻害剤，ポリメラーゼ阻害剤の導入も間近であり，経口薬だけでHCVを撲滅するのも夢ではないと期待できる昨今である。本稿ではHCV増殖系により解明されたHCV生活環を中心に紹介する。

1.HCV培養細胞系確立の試み

1989年ホートンら米国カイロン社のグループにより感染チンパンジーの血漿からHCV遺伝子断片が発見された当時から，C型肝炎患者血清中のHCVを培養細胞に感染させウイルス増殖細胞系を作製する試みが行われてきた。リンパ球系細胞や肝細胞由来細胞株を用いて数多くの感染実験が試みられてきたが，観察できるウイルス量は少なく，ウイルス研究への応用は難しい状況であった。肝細胞を三次元培養すると細胞あたりのアルブミン産生，分泌能や肝特異的薬物代謝酵素の発現が亢進すること，極性細胞の特徴である細胞間ジャンクション構造が形成されることが報告されているので[1]，我々は単層培養系に比べより本来の肝組織に近い立体的な培養環境化の方が肝炎ウイルスの感染増殖に適しているのではないかと期待し，三次元化細胞培養システムであるラジアルフロー型バイオリアクター（RFB）および温度感受性ハイドルゲル（TGP）を利用してHCV培養細胞系の構築を試みた。RFB培養肝細胞株に患者血清を感染，またHCVゲノムcDNAをトランスフェクションし高密度培養を行うことでウイルスの複製増殖を確認した[2]。さらに，遺伝子型1bのダイシストロニックゲノム（全長レプリコン）を保持した細胞株をTGP培養することで，単層培養系では認められなかったウイルス粒子の産生を観察した[3]。しかしながら，依然としてそのHCV増殖レベルは必ずしも高いものではなく，よりウイルス産生効率に優れ，汎用性の高い培養系の開発が待望されていた。

2005年，Wakitaらは東京慈恵会医科大学付属第三病院の劇症肝炎症例の急性期血清からHCV株JFH1を分離した。このクローンを用いて全長のウイルスゲノムRNA合成し，Huh7細胞に導入することにより，ウイルス粒子が産生された[4]。このウイルス粒子は新たなHuh7細胞に感染性を示し，その感染はHCVのエンベロープに対する抗体やHCVの受容体CD81に対する抗体で阻止された。また，培養細胞で作製したウイルスは短期間ながらチンパンジーにも感染した。この系により，ウイルスの感染から分泌までの全ての過程が培養細胞内で解析可能になった。

国立感染症研究所
National Institute of Infectious Diseases（NIID）
〒162-8640　東京都新宿区戸山1-23-1　TEL: 03-5285-1111

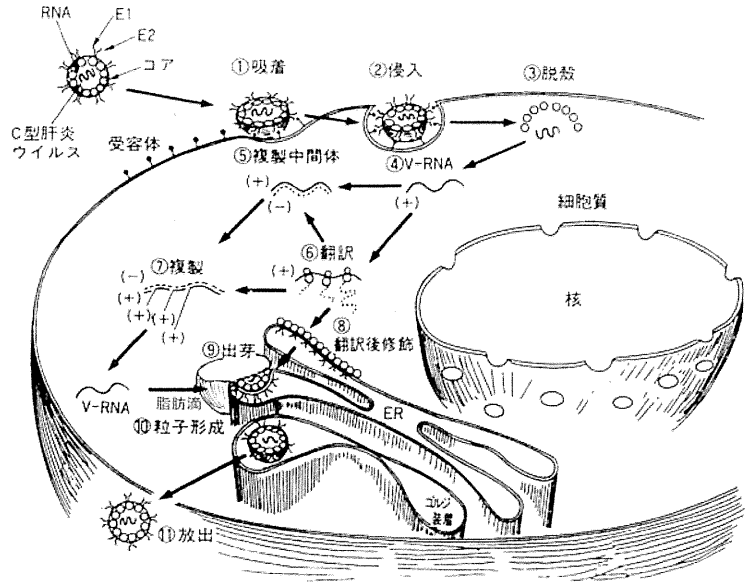

図1　HCVの生活環

2.HCVの生活環

推定されているHCVの生活環を図1に示す。HCVがレセプターを介して肝細胞に吸着，侵入し，粒子よりウイルスRNAが放出され（脱核），これがメッセンジャーRNAとして翻訳され，大きな前駆体蛋白が合成される。この前駆体蛋白は，細胞のシグナラーゼによってウイルス粒子を形成する構造蛋白であるコア蛋白と2つのエンベロープ蛋白E1, E2がプロセスされる。また，ウイルス自身がコードするプロテアーゼによって，プロテアーゼ，ヘリカーゼ，RNA依存性RNAポリメラーゼなどウイルスの複製に必須な非構造蛋白がプロセスされる。ウイルス由来酵素や宿主因子によってゲノムRNAからマイナス鎖RNAが転写され，複製複合体が形成される。これを基にしてプラス鎖RNAが合成され（複製），ウイルスRNAやmRNAとして働く。ウイルスRNAがコア蛋白と結合してヌクレオカプシドを形成し，さらにエンベロープ蛋白が邂逅してERでウイルス粒子が成熟し（出芽），トランスゴルジを通り細胞膜に達して細胞外へ放出されるものと考えられている。以下に各過程について解説する。

（1）吸着と侵入

宿主細胞の受容体とウイルス粒子表面の蛋白の特異性結合はウイルスの組織特異性や宿主域を決定する。HCVは細胞表面に存在するヘパリンやヘパラン硫酸などの硫酸多糖類に捕捉されて濃縮された後，エンベロープ蛋白質を介して親和性の高い蛋白質性受容体に結合し，エンドサイトーシスによってエンドソームに取り込まれる。HCVの感染受容体候補分子として，現在までにHeparansulphate Proteoglycan（HSPG），C型レクチン（DC-SIGN，L-SIGN），Low-Density Lipoprotein（LDL）受容体，CD81，ヒトスカベンジャー受容体クラスB-1型（SR-BI），Claudin-1などが知られている。

（2）翻訳

フラビウイルスやピコルナウイルスなどのウイルスRNAはキャップ構造を持たず，キャップ非依存的なIRESによる翻訳がおこなわれている。HCVでは，40Sリボゾームサブユニットが IRES（38-46番目）に直接結合するところから始まる。ここに，eukaryotic initiation factor（eIF）3などの翻訳開始因子が結合する。IRESに結合する他の宿主因子としては，La蛋白質，heterogeneous ribonucleoprotein L，poly-C binding protein，Pyrimidine Tract-Binding protein（PTB）が知られており，IRES活性の調節に関与している。HCVゲノムの翻訳産物であるポリプロテインは，細胞およびウイルス由来のプロテアーゼにより切断され，成熟した構造および非構造蛋白になる。各構造蛋白質間及びp7/NS2間の切断は宿主細胞小胞体のシグナルペプチダーゼによって行われる。各NS蛋白質間の切断のうち，NS2/NS3間の切断はNS2/NS3金属要求性プロテアーゼにより早期に起こる。一方，NS3からNS5Bの切断はNS3セリンプロテアーゼによる。

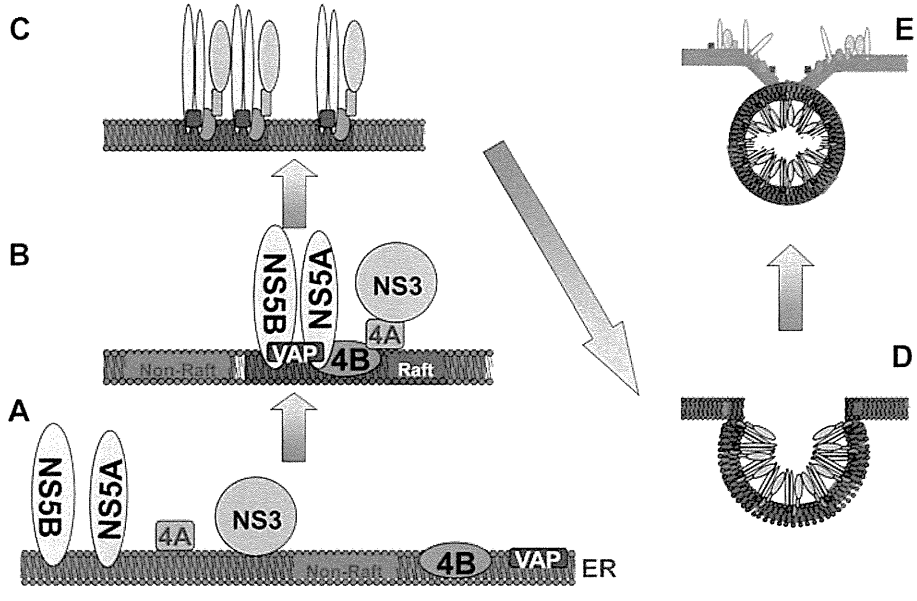

図2　脂質ラフト上でのHCV複製複合体形成モデル

（3）複製

1999年，ドイツのグループは，本来HCVゲノムの中でウイルス粒子を形成する構造タンパク質領域を薬剤耐性遺伝子に置き換え，その下流に，より強力にHCVゲノムの内部から翻訳させる働きを有するEncepharomyocarditis Virus（EMCV）のIRESを挿入したRNAレプリコンを作成した[5]。このRNAをトランスフェクトした細胞を薬剤存在下で培養することで，自律複製するために必要な適応変異を獲得したHCVゲノムと，更にこのHCV遺伝子が複製しうる細胞を選択することを可能にした。レプリコン細胞を電子顕微鏡で観察すると「membranous web」と呼ばれる小胞様構造物が認められることが報告されており[6]，HCVの複製複合体は感染細胞のmembranous webに存在しているものと考えられている。

次に，生化学的手法を用いて，複製活性を維持したままのHCV複製複合体を粗精製し解析したところ，HCV RNAとNS蛋白の大部分は界面活性剤不溶性膜画分（DRM）に残り，HCV RNA複製活性はDRMに検出された[7]。以上のことから，このDRMに複製活性を保持したHCV複製複合体が存在することが判明したことから，HCV複製複合体が脂質ラフト上で形成される可能性が示唆された（図2）。脂質ラフトはコレステロールとスフィンゴ脂質からなると考えられており，HMG-CoAレダクターゼ阻害剤，またはスフィンゴ脂質合成阻害剤が脂質ラフト形成を抑制することで，ウイルス複製を抑えるという報告もあり，脂質ラフトの存在する膜上で複製が起こるという仮説が支持された。HCV複製複合体は脂質ラフトを含む膜小胞構造内に存在し，内部に存在するHCV RNAやNS蛋白は外部からのRNA分解酵素やプロテアーゼに対して保護されているものと考えられた。

（4）粒子形成，分泌

HCV粒子の形成，分泌過程の解析もウイルス培養系の開発により可能となり，脂肪滴の役割が注目されている。Miyanariらはウイルス感染細胞内で脂肪滴をコア蛋白質が被い，さらにそのコア蛋白をNS5A蛋白が被っていることを発見した[8]。NS5A蛋白はER膜上で形成され，脂肪滴上に移行し，そこに存在するコア蛋白と結合していた。コアとNS5A蛋白が結合できない変異をウイルスゲノムに導入すると，感染性ウイルス粒子の形成がなくなったことから，感染性ウイルス粒子の形成には脂肪滴上でのコアとNS5A蛋白質の結合が重要であると考えられた。

脂肪滴周辺で形成されたHCV粒子は，リポ蛋白形成や分泌を抑制すると感染性HCV粒子放出も減少することから，HCVは超低比重リポ蛋白（VLDL）分泌系を利用している可能性が考えられている[9]。HCVゲノムの囲むようにヌクレオキャプシドが形成され，その周りにヘテロダイマーの形成したE1とE2蛋白が覆っている。最近，さらにこの粒子がVLDLや低比重リポ蛋白（LDL）に包まれていることを示す報告が集積してきている。E1とE2にHDL，LDL，